Effect of Vacuum Magnetic Well on Magnetohydrodynamic Stability in Heliotron-E-like Configurations with High Shear

F. Herrnegger

Max-Planck-Institut für Plasmaphysik, IPP-EURATOM Association, Garching bei München

Z. Naturforsch. **42a**, 1085 – 1095 (1987); received July 15, 1987

Dedicated to Professor Dieter Pfirsch on his 60th Birthday

An analysis of $n \geq 1$ free-boundary modes in Heliotron-E-like configurations using the stellarator expansion code STEP is given. It is shown that an axisymmetric quadrupol field improves the stability properties of these high-shear equilibria. The corresponding vacuum quadrupole field is used to find vacuum field configurations with an average magnetic well of $(\Delta V'/V')_{\min} = -4\%$.

1. Introduction

The vacuum magnetic field of the Heliotron-E device [1, 2] is a high-shear $l = 2$ stellarator with a large average magnetic hill, a high rotational transform at the plasma boundary, and a planar magnetic axis. Previous ideal magnetohydrodynamic (MHD) stability computations of free-boundary modes with low values of the toroidal mode number n show that a limiting average β-value of $\langle\beta\rangle_{cr} \approx 2\%$ can be estimated [3 – 6] in agreement with experimental results [1]. In the numerical work a broad pressure profile has been assumed ($\beta_0 \approx 1.35\langle\beta\rangle$). For a more peaked pressure profile the critical $\langle\beta\rangle_{cr}$-value is 1.4%.

As shown in [6], the stabilization of the most unstable $n = 1$, $m = 1$ mode is mainly caused by the increase of shear at the resonant $t = 1$ surface by varying the toroidal field rather than by deepening of the magnetic well. So the critical β-limit increases as the toroidal field increases because the resonant $t = 1$ surface is shifted to the high-shear region. The Heliotron-E device has the feature [6] that within certain limits the toroidal field and thus the twist can be varied. Effects due to the shaping of the pressure profile on the MHD stability have been studied in [3].

In the present paper, the effect of an axisymmetric quadrupole field, which produces a vacuum magnetic well in Heliotron-E-like configurations, on unstable ideal MHD modes in finite-β equilibria is investigated. The asymptotic STEP code [7] was used, being an adequate tool [8 – 10] to study the MHD stability of these equilibria with a free boundary between the plasma and vacuum regions. The exploitation of the vacuum magnetic well as stabilizing mechanism is substantial in low-shear configurations [10 – 12] such as WENDELSTEIN VII-A. In Sect. 2, the equilibrium properties of the Heliotron-E-type configurations being studied are given. In Sect. 3, stability results from the mode analysis and critical β-values are given.

Reprint requests to Dr. F. Herrnegger, Max-Planck-Institut für Plasmaphysik, IPP-EURATOM Association, D-8046 Garching bei München.

2. Vacuum Field Properties and Finite-β Equilibria

The vacuum magnetic field of the Heliotron-E configuration with $M = 19$ field periods around the torus can be approximated in the asymptotic sense [3] by a series of Bessel functions [7] or can be given exactly by Dommaschk potentials [3, 13] as solutions of the Laplace equation. These have been computed for a particular coil field [14] of the Heliotron-E device. In the STEP code an asymptotic representation of these fields is used. Important properties of the magnetic field structure are the radial profiles of the twist t (angle of rotational transform divided by 2π) and the specific volume V' as functions of the toroidal magnetic flux. Other properties [15, 16] associated with the structure of the vacuum magnetic field, such as the magnitude of the Pfirsch-Schlüter currents, are given for a class of configurations.

Using the Bessel model, a standard toroidal stellarator field is given asymptotically in a quasi-cylindrical coordinate system (r, θ, ϕ) by

$$\mathbf{B} = B_0 R_T \cdot \nabla \left[\phi + (\delta/M)\, I_l(Mr/R_T) \sin(l\theta - M\phi)\right],$$

0932-0784 / 87 / 1000-1085 $ 01.30/0. – Please order a reprint rather than making your own copy.

Table 1

Heliotron-E coil field FZH184 MPER, IANP, RA, BZO/IDN, M, L, ANP				
19	40	9.86E−01		−2.879E−03
	2	0	2	1.732E−01
	1	0	3	−2.058E−01
	2	0	4	−6.703E+01
	1	0	5	5.673E+02
	2	0	6	−1.277E+04
	1	19	1	−1.517E−02
	2	19	1	1.476E−02
	1	19	2	−3.224E+00
	2	19	2	−3.170E+00
	1	19	3	1.959E+00
	2	19	3	−4.474E+00
	1	19	4	−1.137E+03
	2	19	4	−5.499E+02
	1	19	5	4.466E+02
	2	19	5	2.308E+02
	1	19	6	−7.947E+04
	2	19	6	1.433E+05
	1	38	1	3.898E−04
	2	38	1	1.800E−04
	1	38	2	−1.612E−02
	2	38	2	4.156E−03
	1	38	3	2.372E+00
	2	38	3	−1.820E+00
	1	38	4	3.984E+02
	2	38	4	4.335E+02
	1	38	5	9.594E+02
	2	38	5	1.602E+03
	1	38	6	5.799E+05
	2	38	6	3.967E+05
	1	57	2	3.494E−03
	2	57	2	2.634E−04
	1	57	3	−1.320E−01
	2	57	3	−1.315E−02
	1	57	4	1.831E+01
	2	57	4	−1.926E−01
	1	57	5	−8.970E+02
	2	57	5	6.319E+02
	1	57	6	−4.554E+04
	2	57	6	−1.502E+05

where R_T is the major torus radius, B_0 the reference field at the magnetic axis, and $I_l(x)$ a Bessel function. For $l=2$, the asymptotic value of the twist on the magnetic axis is given by $t_0 = M\delta^2/16$. A typical value of δ for Heliotron-E is $\delta = 0.67$, giving $t_0 = 0.53$. By applying additional helical $l=3$, 4 fields, the radial profiles of the twist and the specific volume can be changed.

In terms of Dommaschk potentials $V_{m,l}(R,\phi,Z)$, the exact scalar potential for the vacuum field

$$\mathbf{B} = \nabla\left(\phi + \sum_{m,l} V_{m,l}\right),$$

$$m = 0, M, 2M, 3M, \ldots; \quad l = 0, 1, 2, 3, \ldots$$

is given by the Dommaschk functions $D_{m,l}$, $N_{m,l-1}$:

$$V_{m,l}(R,\phi,Z) = A^{(1)}_{m,l} D_{m,l} \sin(m\phi) + A^{(2)}_{m,l} N_{m,l-1} \cos(m\phi) \quad \text{for } l = 0, 2, 4, \ldots,$$

$$V_{m,l}(R,\phi,Z) = A^{(1)}_{m,l} D_{m,l} \cos(m\phi) + A^{(2)}_{m,l} N_{m,l-1} \sin(m\phi) \quad \text{for } l = 1, 3, 5, \ldots,$$

where the notation of [13] is used; here m is a sum index; (R, ϕ, Z) are ordinary cylindrical coordinates, ϕ is the toroidal angle and l the poloidal stellarator mode number; m describes the toroidal harmonics associated with the common period number M; here terms with negative indices must not occur and so $A^{(2)}_{m,l-1} = 0$ for $l = 0$, and because of the stellarator symmetry $V_{m,l}(R,\phi,Z) = -V_{m,l}(R,-\phi,-Z)$, the potential $V_{0,0} = 0$ vanishes.

The normalization used here is that the main toroidal field $B_\phi = 1/R$ is one at $R = 1$. The potential for the homogeneous vertical field B_v in the Z-direction is given by $V^{(1)}_{0,1} = A^{(1)}_{0,1} Z$ (i.e. $D_{0,1} = Z$). The Dommaschk functions $D_{m,l}$, $N_{m,l}$ are explicitly given in [13]. A positive vertical field shifts the mean position of the magnetic axis radially inward. The set of coefficients $A^{(i)}_{m,l}$ for the standard Heliotron-E configuration is given in Table 1 in the last column; here the first two lines name a configuration. In the third line, the number M of field periods, the number of potentials, the average location of the magnetic axis, and the relative size of the homogeneous vertical field (e.g. $B_v/B_0 \approx -0.0029$) are given; the first three columns starting with the fourth line give the upper and the lower indices of $A^{(i)}_{m,l}$.

The potential of the leading $l=2$ stellarator field is given by $A^{(1)}_{19,2}$, $A^{(2)}_{19,2}$. In case of a standard $l=2$ stellarator field, these two coefficients are equal (e.g. $A^{(1)}_{19,2} = C \approx -3.2$ in Table 1). The twist t_0 on the magnetic axis can be obtained from $t_0(M - t_0) = C^2$, and the associated asymptotic value is $t_{asym} = C^2/M$. So the relation of the coefficient C^2 to the amplitude δ in the Bessel model is $C^2 = (M\delta/4)^2$. In the case of Heliotron-E, the period number $M = 19$ is large compared with the twist $t_0 \approx 0.53$ on axis and hence the deviation of the asymptotic t-value from the exact value is very small. A field-line tracing code is also used to compute the twist and the specific volume V'. The Dommaschk coefficients of Table 1 result from the

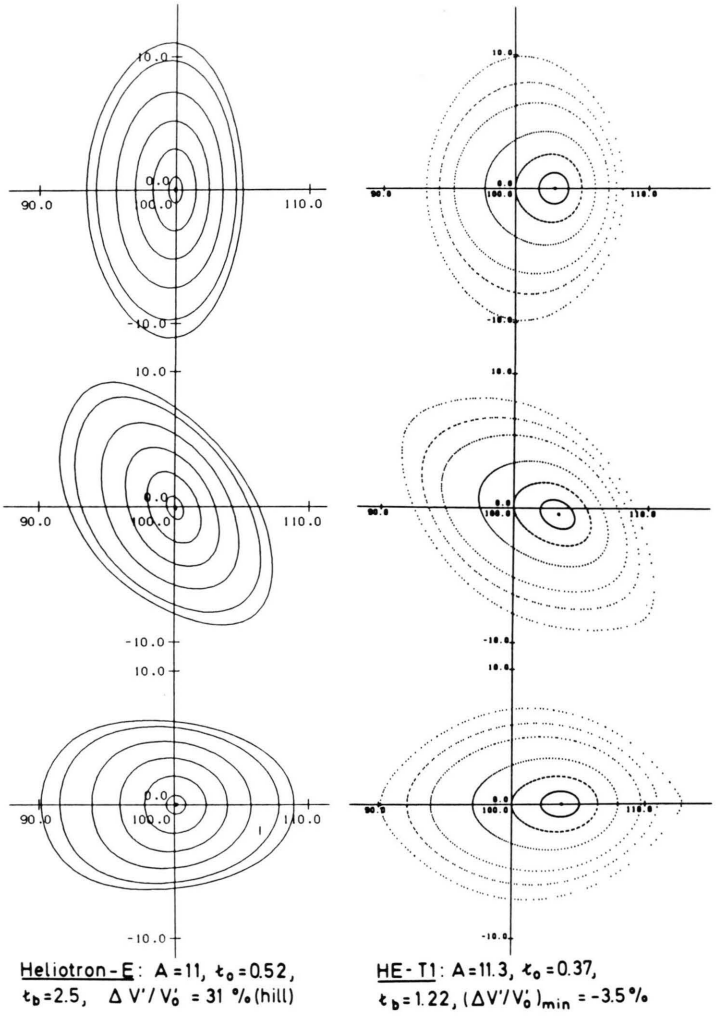

Fig. 1. Contour plots of magnetic surfaces at 0, $L_P/4$, $L_P/2$ of a field period with period length L_P.

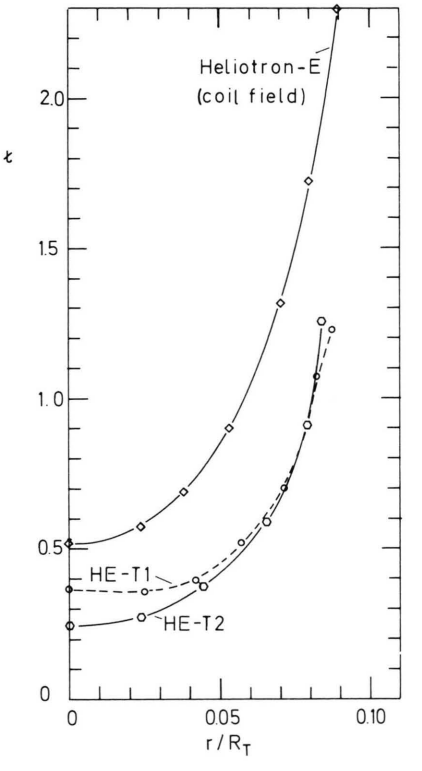

Fig. 2. Twist as function of the minor radius of the magnetic surfaces for the Heliotron-E coil field and the configurations HE-T1, HE-T2.

numerical solution of a boundary value problem [13] to the given vacuum field of a Heliotron-E coil system. For that purpose, the toroidal harmonics up to third order have been included ($m = 57$). In the model fields as given in Tables 2 and 3, only harmonics up to first order ($m = 19$) have been taken into account. The identification of the corresponding Dommaschk potentials ensues from the upper and lower case indices.

The contours of the magnetic surfaces of that configuration are shown in Fig. 1 (left part) at 0, $L_P/4$, $L_P/2$ of a field period with length L_P. The corresponding twist t and the specific volume V', normalized to its value V_0' at the magnetic axis, are shown in Figs. 2 and 3 as functions of the mean minor radius r of the magnetic surfaces, normalized by the major torus radius R_T. The twist profile is approximately

$$t(r) = 0.52\,[1 + 1.30\,(r/a)^2 + 2.23\,(r/a)^4]\,,$$

where a is the mean minor plasma radius and $A = R_T/a$ is the aspect ratio. The Heliotron-E vacuum field has an average magnetic hill of $\Delta V'/V_0' = 31\%$, which is unfavourable for MHD stability, while the high shear provides the stabilization mechanism.

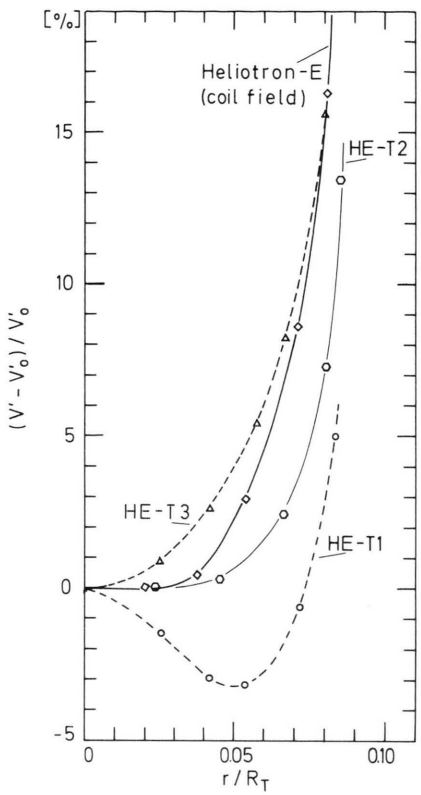

Fig. 3. Specific volume V' as function of r for the Heliotron-E coil field and the configurations HE-T1, HE-T2, HE-T3.

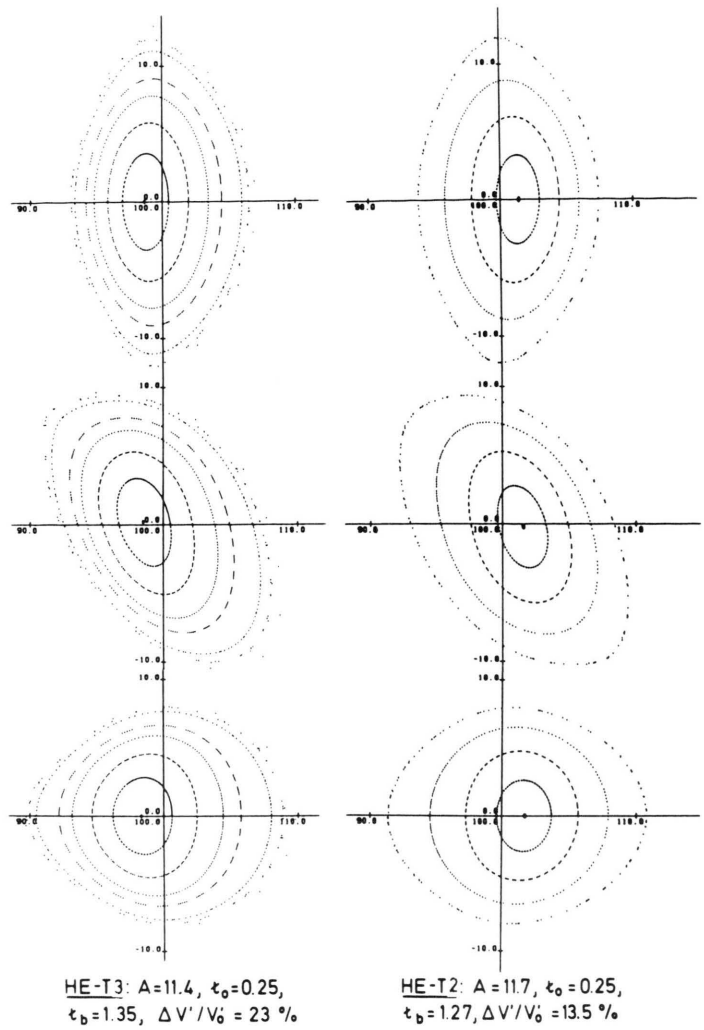

Fig. 4. Contour plots of magnetic surfaces for Heliotron-E like configurations.

To demonstrate how the multipole fields can be adjusted to get a vacuum field configuration with an average magnetic well ($V'' < 0$), three different configurations are shown in the Figs. 1 and 4 (the corresponding potentials are given in Table 2). Fields of this type are then used to perform the mode analysis. Essentially, the homogeneous vertical field, the axisymmetric quadrupole ($A^{(2)}_{0,2}$) and hexapole ($A^{(1)}_{0,3}$) fields have been adjusted to get configurations with good field properties. The homogeneous vertical field can be used to shift the plasma column radially inward, but at the same time the average magnetic hill is increased. A helical dipole field ($A^{(1)}_{19,1}, A^{(2)}_{19,1}$) is therefore applied [10] to shift the plasma column radially inward (towards the main torus axis) and outward, which does not displace the magnetic surfaces to each other.

The twist t and the specific volume V' of the Heliotron-E-like configurations HE-T1, HE-T2, HE-T3 are shown in the Figs. 2 and 3 as functions of r/R_T. The t-profile of the configuration HE-T1

Table 2

Field configuration HE-T1
MPER, IANP, RA, BZO/IDN, M, L, ANP

19	13	1.00E + 00		−0.006E + 00
	2	0	2	−0.120E + 00
	1	0	3	−0.090E + 00
	1	19	2	−1.920E + 00
	2	19	2	−2.520E + 00
	1	19	3	−5.580E + 00
	2	19	3	+6.480E + 00
	1	19	4	−6.480E + 02
	2	19	4	−3.120E + 02
	1	19	5	−3.258E + 03
	2	19	5	2.916E + 03
	1	19	6	−2.004E + 05
	2	19	6	−5.604E + 04

Field configuration HE-T2
MPER, IANP, RA, BZO/IDN, M, L, ANP

19	13	1.00E + 00		−0.006E + 00
	2	0	2	+0.120E + 00
	1	0	3	−0.090E + 00
	1	19	2	−1.920E + 00
	2	19	2	−2.520E + 00
	1	19	3	−5.580E + 00
	2	19	3	+6.480E + 00
	1	19	4	−6.448E + 02
	2	19	4	−3.120E + 02
	1	19	5	−3.258E + 03
	2	19	5	2.916E + 03
	1	19	6	−2.004E + 05
	2	19	6	−5.604E + 04

Field configuration HE-T3
MPER, IANP, RA, BZO/IDN, M, L, ANP

19	13	1.00E + 00		+0.006E + 00
	2	0	2	+0.120E + 00
	1	0	3	+0.090E + 00
	1	19	2	−1.920E + 00
	2	19	2	−2.520E + 00
	1	19	3	−5.580E + 00
	2	19	3	+6.480E + 00
	1	19	4	−6.480E + 02
	2	19	4	−3.120E + 02
	1	19	5	−3.258E + 03
	2	19	5	2.916E + 03
	1	19	6	−2.004E + 05
	2	19	6	−5.604E + 04

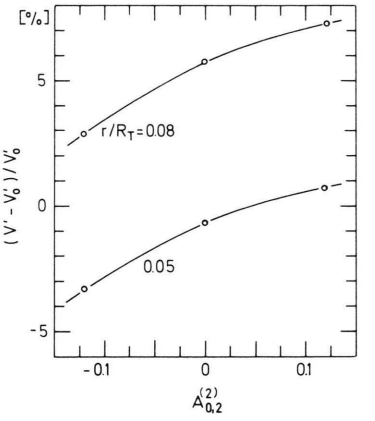

Fig. 5. Normalized specific volume as function of the axisymmetric quadrupole field at various minor radii for the configurations HE-T1 and HE-T2.

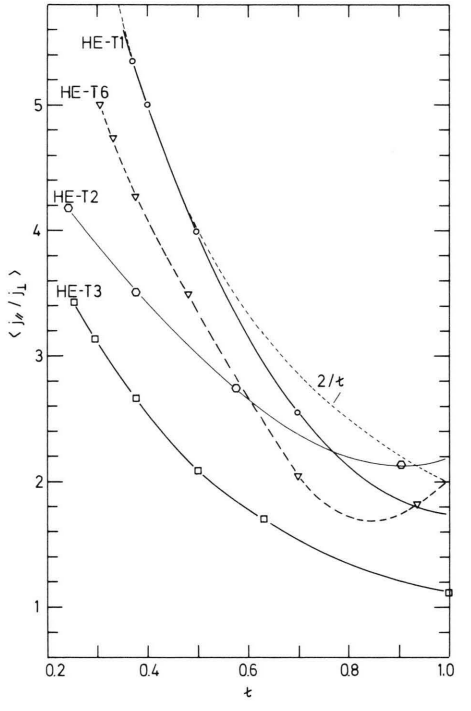

Fig. 6. Normalized parallel current density as function of the twist t for various configurations.

is very flat near the magnetic axis. The twist and global shear $\Delta t/t_0$ are somewhat smaller than for the Heliotron-E coil field, but the local shear rt'/t is large near the plasma boundary where the $n = 1$, $m = 1$ mode is resonant to $t = n/m = 1$; here m and n are the mode numbers of instabilities in the poloidal and toroidal directions, respectively.

For the stability analysis (Sect. 3), the t-range is chosen such that the mode with $n/m = 1$ is resonant to $t = 1$ within the plasma region, where the

shear is small near the magnetic axis in the finite-β configurations. The specific volume V' decreases to values of $\Delta V'/V'_0 = -3.5\%$ (at $r/a \approx 0.6$, see Fig. 3) as the minor radius increases and only in the outer plasma region the quantity V'' is positive. A negative V'' is favourable for MHD stability. In the case of high t-values at the boundary ($t_b \approx 2$), V'' is negative only in a very narrow region near the magnetic axis. The dependence of the magnetic well on the axisymmetric quadrupole field is shown in Fig. 5, where the normalized specific volume is plotted as function of $A^{(2)}_{0,2}$ for two different magnetic surfaces (labelled by the normalized minor radius r/R_T). For $A^{(2)}_{0,2} = -0.15$, the average magnetic well is about -4% at $r/R_T = 0.05$. All results shown in the Figs. 1 to 6 are vacuum field properties and have been computed by a field-line tracing code.

Another quantity of interest for Advanced Stellarators [15] is the magnitude of the normalized parallel current density, which is measured by $\langle j_\parallel / j_\perp \rangle$ and depends sensitively on the quadrupole field. The ration $\langle j_\parallel / j_\perp \rangle$ is obtained from the poloidal variation of $\int dl/B$ of the vacuum magnetic fields, taken along a field line over one field period. The quantities $j_\parallel$ and $j_\perp$ are the absolute values of the secondary and the diamagnetic current densities, respectively. This quantity scales as $2/t$ for a standard $l = 2$ stellarator. This is shown in Fig. 6 for the various configurations. The configuration HE-T3 has the remarkable feature that the Pfirsch-Schlüter currents are considerably reduced but, unfortunately, the twist at the magnetic axis is small and a high average magnetic hill of the same order as for the coil field of Heliotron-E appears. This is a common feature with other reduced-Q configurations [17]. Since the Pfirsch-Schlüter currents are considerably reduced here and are of the order of those in the W VII-AS configuration, it is of interest to study this effect on global unstable modes.

The stellarator expansion procedure STEP [7] reduces the finite-β equilibrium problem to solution of a two-dimensional elliptic differential equation of the Grad-Schlüter-Shafranov type for the average normalized poloidal flux function ψ. The input data consist of two free functions of ψ, namely the pressure $p(\psi)$ and the toroidal net current in each flux surface (or equivalently the twist profile), together with the vacuum magnetic field data averaged over one field period. All equilibria studied here are net-current-free stellarators and consequently the twist profiles result accordingly.

An inherent feature of the asymptotic representation of vacuum fields is that the shear and the average magnetic well depth are somewhat smaller than it results from exact integration of magnetic field lines [9]. The pressure profile $p(\psi)$ is assumed to be $p(\psi) = p_0(1-\psi)$, resulting in an approximately parabolic pressure profile in r. So the relation between the average $\langle \beta \rangle$-value and the β_0-value at the magnetic axis is approximately $\langle \beta \rangle \approx \beta_0/1.7$. In all cases the aspect ratio is about $A = R_T/a \approx 11$.

In the asymptotic theory, the magnetic surfaces of lowest order are axisymmetric. The contours of the lowest-order magnetic surfaces of a typical finite-β equilibrium configuration are shown in Fig. 7 for $\langle \beta \rangle = 2.2\%$ ($\beta_0 = 3.7\%$, upper graph), as computed by the STEP code. A free boundary between the plasma and vacuum regions is assumed. The associated Dommaschk potentials are given in Table 3 (configuration HE-T4). For comparison, the corresponding vacuum field configuration ($\beta = 0$) is also shown in the lower graph of Figure 7.

The contours of the plasma boundary are almost the same for $\langle \beta \rangle = 0$ and 2.2%. The effect of the negative quadrupole field (axisymmetric $l = 2$ field) is clearly observed near the magnetic axis (lying ellipses). At high β-values these lying ellipses were changed to standing ellipses. As shown in Sect. 3, the stability properties of the finite-β con-

Table 3.

Field configuration HE-T4 MPER, IANP, RA, BZO/IDN, M, L, ANP				
19	15	1.00E+00		−0.012E+00
	2	0	2	−0.170E+00
	1	0	3	+0.100E+00
	1	19	1	−0.020E+00
	2	19	1	+0.020E+00
	1	19	2	−3.100E+00
	2	19	2	−3.400E+00
	1	19	3	−2.540E+01
	2	19	3	+2.990E+01
	1	19	4	−6.480E+02
	2	19	4	−3.120E+02
	1	19	5	−3.258E+03
	2	19	5	2.916E+03
	1	19	6	−2.004E+05
	2	19	6	−5.604E+04

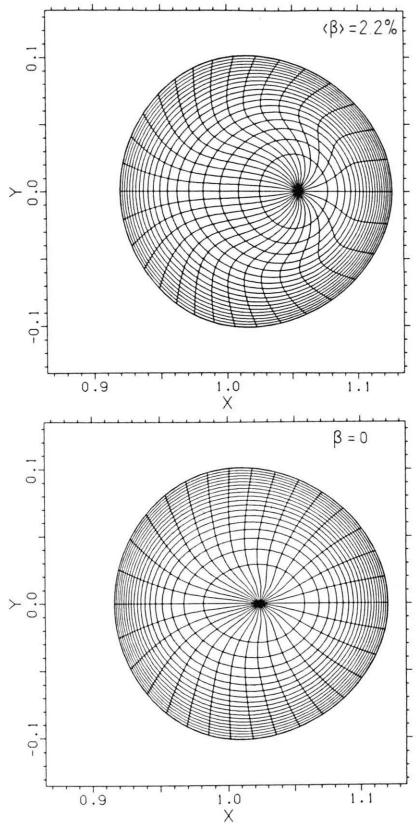

Fig. 7. Contours of zeroth-order magnetic surfaces of the configuration HE-T4 (Table 3).

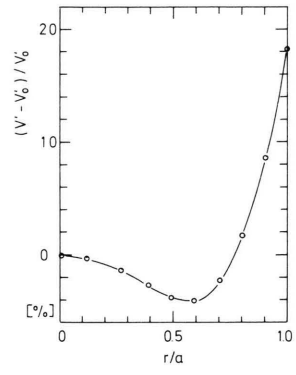

Fig. 8. Normalized specific volume as function of the minor radius for the configuration HE-T4 with $\langle\beta\rangle = 2.2\%$.

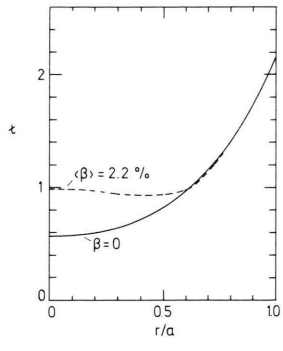

Fig. 9. Twist as function of the minor radius at various β-values in the configuration HE-T4.

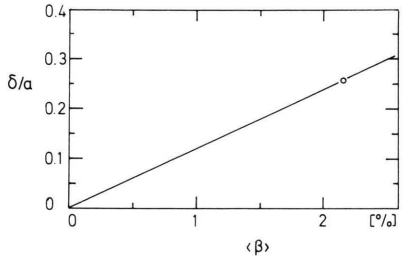

Fig. 10. Shafranov displacement of the magnetic axis as function of $\langle\beta\rangle$ for the configuration HE-T4.

figurations are improved if the axisymmetric quadrupole field at $\beta = 0$ takes even larger absolute values than used here. This stabilizing mechanism is the same as creating an average magnetic well in the vacuum field by applying an axisymmetric quadrupole field (see Figure 5). For comparison, the contours of the zeroth order magnetic surfaces of the standard Heliotron-E configuration are standing ellipses as can be observed from Figure 1.

Figures 8 and 9 show the specific volume V' and the twist as functions of the minor plasma radius for the configuration HE-T4 with $\langle\beta\rangle = 2.2\%$. The twist profile is changed at finite β only in the interior plasma region ($r/a \leqslant 0.5$), but is the same in the outer region. Although the twist at finite β is very close to one in the interior plasma region and thus is resonant with $n/m = 1$ modes, no unstable modes with low toroidal mode numbers $n = 1$ to 5 were observed. The reason is that the magnetic well (see Fig. 8) near the magnetic axis is sufficiently deep to stabilize these modes. The finite-β Shafranov displacement δ/a is shown in Fig. 10 as function of $\langle\beta\rangle$.

3. Stability Results, Critical β

The analysis of free-boundary modes was performed for the Heliotron-E coil field configuration (Table 1) and the model fields HE-T1 to HE-T4 (Tables 2 and 3), where the axisymmetric quadrupole and the helical dipol fields were varied. The helical $l = 2$ field ($A^{(1)}_{19,2}$) is adjusted so that the twist at the boundary assumes the desired value. The equilibrium density profile ϱ is determined from the equilibrium pressure by $\varrho \sim \sqrt{p}$ where the density at magnetic axis is one (i.e. the adiabatic exponent $\gamma^* = 2$). Together with the reference

magnetic field B_0 that determines the Alfvén velocity v_A, which is used to normalize the eigenvalue $(\gamma R_T/v_A)^2$. If negative eigenvalues occur, the configuration is unstable. The numerical procedure STEP to solve the eigenvalue problem is described in [7]. In all examples here, there is a vacuum region surrounding the plasma. An electrically conducting wall is assumed to be at infinity.

An unstable eigenfunction is represented by the Fourier components η_m of the stream function η such that $\xi = \nabla\phi \times \nabla\eta$ and by the arrow plot of the displacement vector ξ where the length of the arrow measures the relative magnitude of the displacement vector. Figure 11 shows an example of an unstable $n = 1$ free-boundary mode (upper graph), where only the dominant $m = 1$ Fourier harmonic and its neighbouring side bands have a sizable amplitude. The eigenfunction assumes its maximum at the boundary (external free-boundary mode). The lower graph shows the corresponding displacement vector. The eigenvalues and the twist at the magnetic axis and at the boundary are given in the Figures.

In Fig. 12, an unstable $n = 4$ free-boundary mode is shown. The t-profile of the equilibrium configuration is chosen such that the main resonances $n/m = 1$ and $n/m = 4/3$ are within the plasma region. Both resonances appear on those magnetic surfaces where the resonance condition, $t_{res} = n/m$, is satisfied. In configurations with higher shear, other Fourier harmonics can be resonant. An unstable eigenfunction with several resonant Fourier harmonics is shown in Fig. 13, where the finite-β equilibrium configuration is similar to the configuration HE-T3 and is chosen such that $t_0 = 0.47$, $t_b = 1.79$, which results in a high shear near the magnetic axis. In this case, however, the shear stabilization is not sufficient to stabilize these modes. At the same time it is shown that the fine radial structure of the modes can be resolved.

For the standard Heliotron-E coil field, the eigenvalues of the most unstable $n = 2$, $m = 2$ free-boundary mode is computed as function of $\langle\beta\rangle$. This is shown in Fig. 14, where the critical $\langle\beta\rangle_{cr}$-value is found to be $\langle\beta\rangle_{cr} = 1.4\%$ for the pressure profile $p = p_0(1-\psi)$. This result agrees with that found by Johnson [3]. No unstable free-boundary modes with toroidal mode numbers $n = 1$ to 5 investigated so far have been found at smaller β-

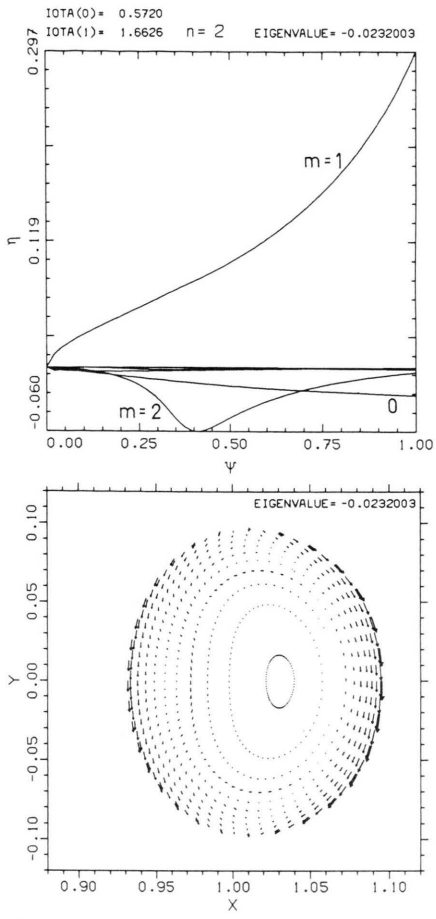

Fig. 11. Unstable $n = 2$ eigenfunction with dominant $m = 1, 2$ Fourier harmonics (upper graph) and displacement vectors (lower graph, $\beta_0 = 3\%$, $\langle\beta\rangle = 1.8\%$).

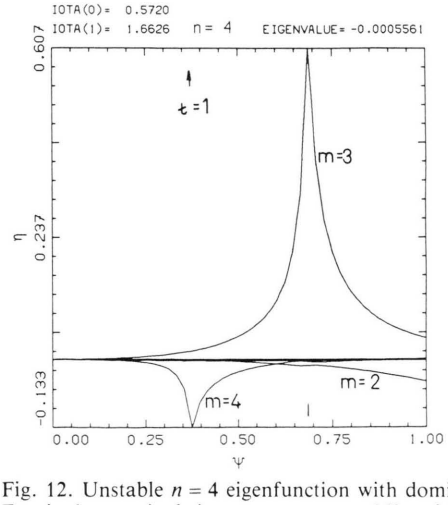

Fig. 12. Unstable $n = 4$ eigenfunction with dominant $m = 3, 4$ Fourier harmonics being resonant at $t = 4/3$ and $4/4$ ($\beta_0 = 3\%$, $\langle\beta\rangle = 1.8\%$).

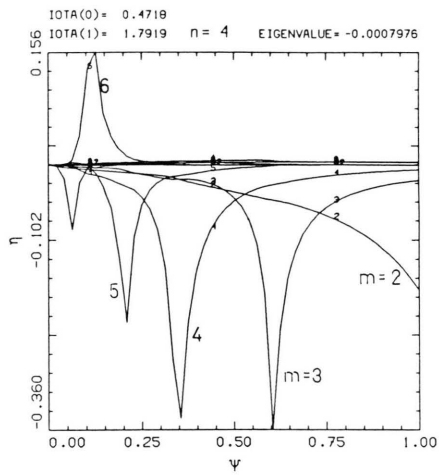

Fig. 13. Unstable $n = 4$ eigenfunction with several resonant Fourier harmonics in a high shear system.

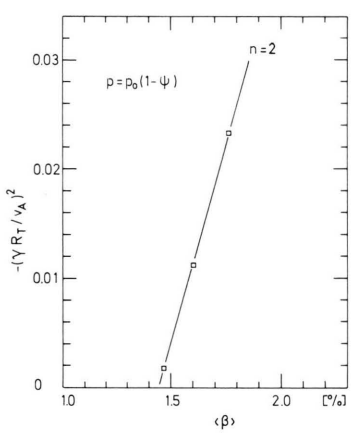

Fig. 14. Normalized eigenvalues of an unstable $n = 2$ free-boundary mode as function of $\langle\beta\rangle$ in the Heliotron-E experimental device.

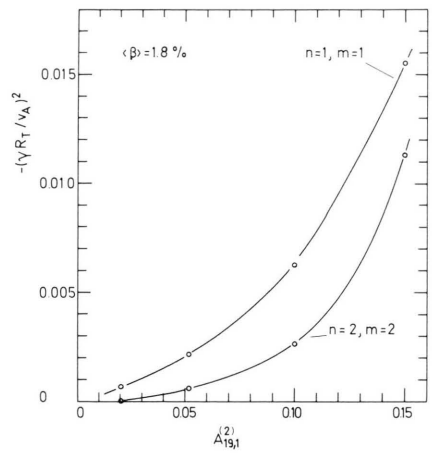

Fig. 15. Eigenvalues of $n = 1$ and $n = 2$ modes as functions of the helical dipole field.

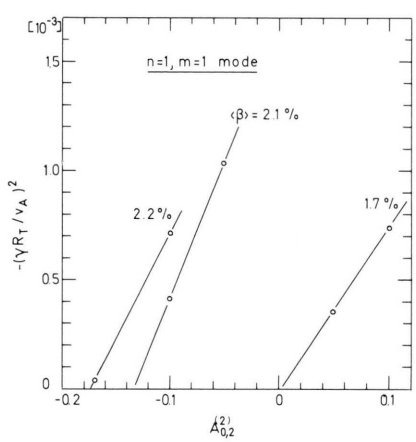

Fig. 16. Eigenvalues of $n = 1$, $m = 1$ modes as functions of the axisymmetric quadrupole field for several $\langle\beta\rangle$-values.

values. At higher β-values, other modes with $n = 3, 4, 5$ are found to be unstable.

To improve the stability properties of this class of equilibria at higher β-values, the helical dipole field ($A^{(1)}_{19,1} = -A^{(2)}_{19,1}$) was varied. In general, each of these potentials can be varied independently. The results for the eigenvalues of unstable modes are shown in Figure 15. The Dommaschk potentials of the corresponding equilibrium configuration are the same as given in Table 3 except $A^{(1)}_{19,2} = -3.0$, $A^{(2)}_{19,2} = -3.6$, $A^{(2)}_{0,2} = 0.1$; $A^{(2)}_{19,1}$ is varied between 0.02 and 0.15, which results in a small change of the twist profile $t_0 = 0.68$ ($t_b = 1.89$) to $t_0 = 0.78$ ($t_b = 2.1$), respectively. Here, one observes that the magnitude of the most unstable eigenvalue is diminished by more than one order of magnitude.

However, the axisymmetric quadrupole field ($A^{(2)}_{0,2}$) is more effective in removing the remaining resonant unstable modes, as is shown in Figure 16. The equilibrium configuration is the same as given in Table 3 except $A^{(1)}_{19,2} = -3.3$, $A^{(2)}_{19,2} = -3.6$; the

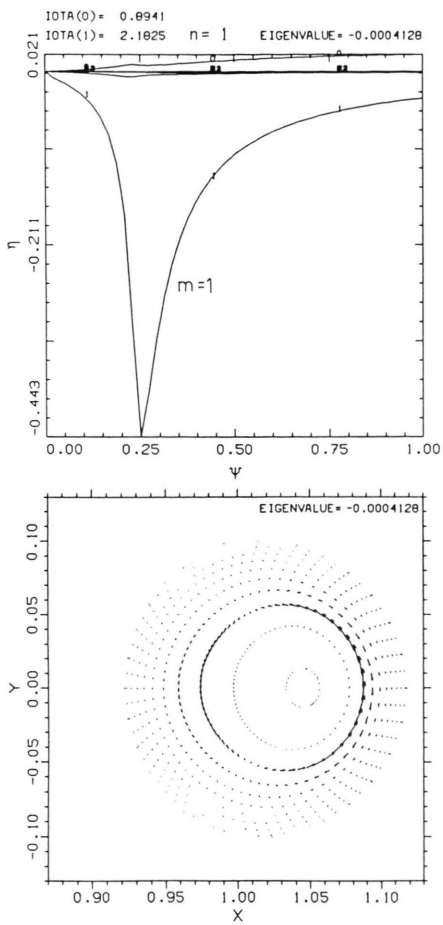

Fig. 17. Internal $n = 1$, $m = 1$ free-boundary mode and displacement vector.

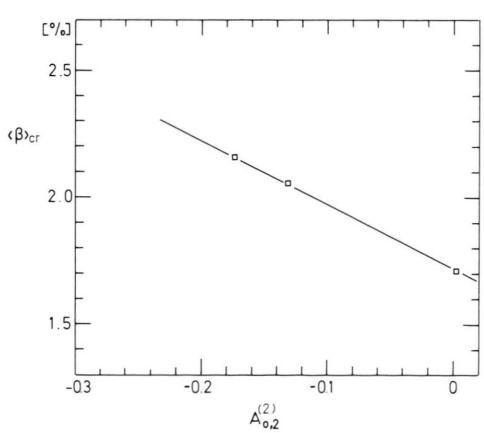

Fig. 18. Critical β-value as function of the quadrupole field for stable Heliotron-E-like configurations.

axisymmetric quadrupole field ($A^{(2)}_{0,2}$) is varied within a certain range. Here the eigenvalues of unstable $n = 1$, $m_{res} = 1$ modes are plotted as functions of $A^{(2)}_{0,2}$ for various $\langle\beta\rangle$-values. The same study has been carried out for $n = 2, \ldots, 5$ modes. In all configurations of this class, no unstable free-boundary modes with $n = 1$ to 5 were found after the $n = 1$, $m = 1$ resonant mode had been stabilized. The structure of this internal free-boundary mode and the displacement vectors are shown in Figure 17.

The equilibrium configuration HE-T4 (see Table 3) with $\langle\beta\rangle = 2.2\%$ is shown in Fig. 7, where all low n modes have been stabilized. The scaling of the critical $\langle\beta\rangle_{cr}$-value for stability with the quadrupole field is shown in Figure 18. For this class of high-shear magnetic field configurations, the critical $\langle\beta\rangle_{cr}$-value for MHD stability was increased from 1.4% to $\langle\beta\rangle_{cr} = 2.2\%$. Applying a broader pressure profile with zero pressure gradient at the boundary and using even larger quadrupole fields, the critical β-value can be improved. A second stability regime for free-boundary modes was not found.

4. Conclusions

It is shown that for Heliotron-E-like configurations, an axisymmetric quadrupole field allows the independent control of the vacuum magnetic well in a broad region near the magnetic axis and improves the critical beta-values for stability resulting from an ideal MHD stability analysis of free-boundary modes. It is worth-while to consider the realization of such magnetic field configurations in the existing Heliotron-E device or in the next large helical device of MOE (Ministry of Education, Science, and Culture of Japan) being designed by the Heliotron group in Kyoto, the Institute of Plasma Physics in Nagoya, and other groups. It also offers a way to investigate experimentally effects of the Pfirsch-Schlüter currents in existing experimental devices. Effects of axisymmetric quadrupole fields in the WENDELSTEIN VII-A and VII-AS configurations will be studied.

Acknowledgements

The author wishes to thank Dr. John L. Johnson for providing the STEP code and for many encouraging and critical remarks.

[1] K. Uo, Nucl. Fusion **25,** 1243 (1985).
[2] M. Wakatani, K. Ichiguchi, H. Sugama, K. Itoh, A. Hasegawa, J. Todoroki, and H. Naitou, Plasma Physics and Contr. Nuclear Fusion Res. 1986, Paper IAEA-CN-47/D-V-3 (Kyoto, 11th Conference, Nov. 1986, IAEA Supplement 1987, Vienna).
[3] G. Rewoldt and J. L. Johnson, Plasma Phys. Contr. Fusion **27,** 1203 (1985). – J. L. Johnson and G. Rewoldt, in the Proc. Intern. Workshop on Stellarators/Heliotron, Vol. 2, p. 330, Nov. 1986, Kyoto, Japan. – G. Rewoldt, M. Wakatani, and J. L. Johnson, Plasma Phys. Contr. Fusion **29** (1987).
[4] M. Wakatani, K. Ichiguchi, F. Bauer, O. Betancourt, and P. R. Garabedian, Nucl. Fusion **26,** 1359 (1986).
[5] F. Sano, Y. Takeiri, M. Murakami, et al., in the Proc. Intern. Workshop on Stellarators/Heliotron, Nov. 1986, Kyoto, Japan.
[6] B. A. Carreras, L. Garcia, and V. E. Lynch, Phys. Fluids **29,** 3356 (1986).
[7] G. Anania, J. L. Johnson, and K. E. Weimer, Phys. Fluids **26,** 2210 (1983). – G. Anania and J. L. Johnson, Phys. Fluids **26,** 3070 (1983).
[8] F. Herrnegger, P. Merkel, and J. L. Johnson, J. Comput. Physics **66,** 445 (1986).
[9] F. Herrnegger, 5th Intern. Workshop on Stellarators, Vol. I, p. 401; Commission of the Europ. Comm. CEC, Brussels, Belgium; F. Rau and G. G. Leotta, Eds., EUR 9618 EN, 1984.
[10] F. Herrnegger, Magnetohydrodynamic Stability Analysis of Wendelstein VII-A Equilibria, to be published.
[11] F. Herrnegger, 14th Europ. Conf. on Contr. Fusion and Plasma Physics, ECA Vol. **11D,** Pt. I, p. 419 (22 – 26 June 1987, Madrid, Spain; Europ. Phys. Soc., F. Engelmann and J. L. Alvarez Rivas, Eds.).
[12] F. Herrnegger, Z. Naturforsch. **37a,** 879 (1982).
[13] W. Dommaschk, Z. Naturforsch. **36a,** 251 (1981) and **37a,** 867 (1982). – Comput. Phys. Comm. **40,** 203 (1986).
[14] F. Rau, Private Communication 1984.
[15] R. Chodura, W. Dommaschk, F. Herrnegger, W. Lotz, J. Nührenberg, and A. Schlüter, IEEE Trans. Plasma Sciences **PS-9,** 221 (1981). – A. Schlüter, Nucl. Instrum. Meth. Physics Res. **207,** 139 (1983).
[16] F. Herrnegger and F. Rau, 13th Europ. Conf. on Contr. Fusion and Plasma Heating (Schliersee, April 1986), ECA Vol. 10C, Pt. I, p. 307 (Europ. Phys. Soc. 1986, G. Briffod and M. Kaufmann, Eds.).
[17] F. Rau and W. Lotz, W VII-A Team, 9th Europ. Conf. on Contr. Fusion and Plasma Physics, Vol. 1, p. 76, Oxford 1979, England.